Chinese Chemical Letters 37 (2026) 111598

Contents lists available at ScienceDirect

Chinese Chemical Letters

journal homepage: www.elsevier.com/locate/cclet

A robust nonfouling electrochemical biosensor with both filtering and antifouling strategies for cortisol detection in human blood

Xiujuan Qiao, Rui Han, Xinru Xu, Mingrui Lv, Yiting Hou, Xiliang Luo*

Key Laboratory of Optic-electric Sensing and Analytical Chemistry for Life Science, MOE, Shandong Key Laboratory of Biochemical Analysis, College of Chemistry and Molecular Engineering, Qingdao University of Science and Technology, Qingdao 266042, China

ARTICLE INFO

Article history:
Received 19 December 2024
Revised 7 June 2025
Accepted 16 July 2025
Available online 17 July 2025

Keywords:
Nonfouling
Electrochemical biosensor
Size-sieving
Polypeptide complex hydrogel
Cortisol
Human blood

ABSTRACT

The heavy biofouling on electrochemical sensor surface poses a formidable challenge for biosensing in human blood. Herein, we designed a multilayer filtering-sensing sandwich patch that served as a versatile platform to surmount the substantial fouling constraints for detection in human blood. The patch integrated two functional layers: (i) Inspired by dialysis phenomenon, a filtering-mass transfer hydrophilic membrane with heterogeneous nanostructure was used to filter large-size substances (like cells, bacteria and microorganisms, *etc.*) and continuously pass through the rest of the biological fluid (like proteins, metabolites and inorganic salts, *etc.*). (ii) the polypeptide composite hydrogel (rGO/PEPG) on the screen-printed electrode (SPE) surface, with the modulation of -COOH and -NH_2 groups, endowed a strong hydrophilic layer with electric neutrality to further facilitate the antifouling ability. Notably, the integration of the filtering porous membrane with the antifouling hydrogel ensures the strong antifouling ability of the electrochemical sensor in complex human blood. Furthermore, the self-healing property of the rGO/PEPG, relying on the physical π-π stacking forces, aligns the electrochemical sensor with practical needs. The constructed antifouling biosensor based on the filtering-sensing sandwich patch was successfully applied for the sensitive detection of cortisol in human blood, with an acceptable accuracy comparable to the enzyme-linked immunosorbent assay (ELISA) method. The strategy presented herein represent a promising advance along the road to construct effective antifouling biosensing devices with robust operation in diverse complex body fluids.

© 2025 Published by Elsevier B.V. on behalf of Chinese Chemical Society and Institute of Materia Medica, Chinese Academy of Medical Sciences.

Electrochemical sensors are highly promising for biomedical diagnostics, offering advantages such as exceptional sensitivity, precise selectivity, easy miniaturization, affordability, and straightforward operation [1–7]. However, the substantial biofouling present in complex human blood poses a significant challenge for *in-situ* biosensing [8–10]. Regularly, the electrode surface may experience persistent and strong adhesion from various complex substances in human fluid systems, including cells, proteins and other compounds. Such biofouling may hamper electrode functionality, leading to decreased sensitivity and reliability [11,12].

Moreover, achieving accurate sensing in human blood remains a challenge. For example, direct application of immunoassays to blood samples may potentially lead to cell damage or lysis, compromising the validity of the assay outcomes [13]. Currently, traditional blood assay methods [14] require serum extraction from blood through a pretreatment process [14,15]. Furthermore, the time-consuming nature of the pretreatment process raises concerns about potential delays in obtaining assay results. Even with certain commercial devices featuring individual blood separation units, achieving real-time and online blood analyses remain a formidable challenge [16]. Similarly, the direct use of electrochemical sensors in human blood poses challenges. Hence, it is crucial to develop electrochemical sensors with strong biofouling resistance to effectively minimize interferences in complex human blood samples.

Dialysis phenomenon is one of the physiological functions of the kidney *in vivo* [17]. The inner wall of the renal glomerulus features a filtration membrane composed of numerous narrow filtration slits. As capillaries deliver plasma to the renal glomerulus, it undergoes filtration through this membrane. Components like water, electrolytes, small organic molecules, and drugs in the blood are filtered into the renal tubules with the help of diffusion effect. However, large molecules such as blood cells and proteins are unable to pass through the filtration membrane. Inspired by the filtering function of dialysis phenomenon, membrane separation technology shows potential for blood purification (called hemodialysis) [18], where toxins are removed from the blood through a mem-

* Corresponding author.
E-mail address: xiliangluo@qust.edu.cn (X. Luo).

https://doi.org/10.1016/j.cclet.2025.111598
1001-8417/© 2025 Published by Elsevier B.V. on behalf of Chinese Chemical Society and Institute of Materia Medica, Chinese Academy of Medical Sciences.

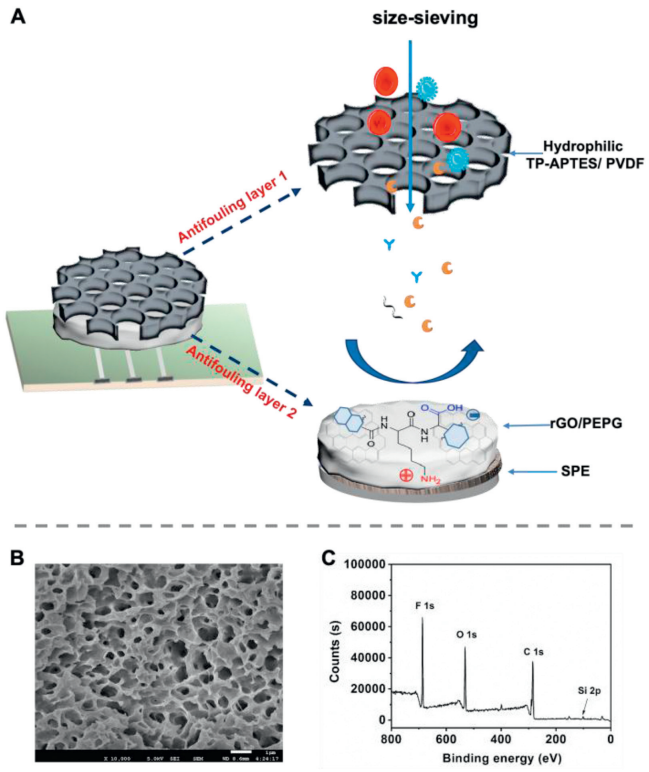


Fig. 1. (A) The schematic diagram for the enhanced antifouling performance principle of the filtering-sensing sensor patch. (B) The scanning electron microscope (SEM) and (C) X-ray photoelectron spectroscopy (XPS) of TP-APTES/PVDF.

brane. Hemodialysis treatment is a common method for patients suffering from irrecoverable kidney damage. Through a mechanism similar to hemodialysis, porous membranes might have the potential for antifouling functions for biosensing in human blood.

In addition, widely acknowledged is the understanding that biofouling primarily arises from the non-specific adsorption of cells, proteins, and other substances. Materials endowed with extreme hydrophilicity, when modified on electrode surfaces, typically thwart the undesired adhesion of these complex contaminants [19–24], such as polyampholytes, poly(ylides), and polybetaines [25–27]. Among them, polypeptides have recently gained popularity in biomedical applications due to their positive and negative groups, high biocompatibility, the easy modulation of specific functional groups, and its structure [28,29]. Remarkably, its great hydrophilicity causes hydrophilic layer forming, alleviating non-specific adhesion onto electrode interfaces, which contributes to the construction of low-fouling biosensors [28]. Hydrogels, characterized by their inherent advantages of hydrogel natural hydration layer structure, three-dimensional (3D) structure, and flexibility, have consistently been the focus of research for the preparation of antifouling electrochemical sensors [30,31]. Polypeptides based hydrogel (PEPG) thus will facilitate the antifouling performances for *in situ* biosensing.

In response to the formidable challenge of heavy biofouling in complex human blood, we present a robust antifouling filtering-sensing strategy implemented within a multilayer sandwich patch. This approach incorporates two functions to surmount the substantial fouling constraints (Fig. 1A). A porous membrane of tea polyphenols and 3-aminopropyltriethoxysilane modified polyvinylidene fluoride (TP-APTES/PVDF) with a heterogeneous and hydrophilic nanostructure was employed to facilitate the continuous filtration of micrometer-sized contaminants (like cells, bacteria and microorganisms) while allowing biological fluid to pass through its channels (filtering-mass transfer porous membrane, Fig. 1B). The porous TP-APTES/PVDF layer is hydrophilic and serves as the antifouling or filtering layer 1. The peaks of F 1 s, O 1 s, C 1 s, Si 2p in Fig. 1C demonstrated the successful modification of TP-APTES on the PVDF membrane. In addition, an antifouling PEPG containing reduced graphene oxide (rGO) was applied to modify the screen-printed electrode (SPE) to further improve the antifouling ability of the sensing system. Peptide of 2-Nap-K-(2-Nap)-KF (The structure in Fig. S1 in Supporting information) based hydrogel serves as the antifouling layer 2, initially designed with -COOH and -NH_2 with extreme hydrophilia and electric neutrality, forms an antifouling membrane on electrochemical sensors surface to alleviate nonspecific adhesion. Two Nap groups and 2 dimensions (2D) rGO here act as a key contribution to prepare rGO/PEPG. They are chosen to provide the stronger π-π stacking force to create a self-healing peptide complex hydrogel rGO/PEPG. Significantly, the integration of these two strategies holds the potential to substantially enhance antifouling capability of the biosensor for the sensitive cortisol detection in blood.

The experimental procedures were outlined in the Supporting information.

To introduce microcellular structure into the PVDF layer, PVDF macromolecules were mixed with hydrophilic polyethyleneglycol (PEG-6000) in *N*,*N*-dimethylacetamide (DMAc) with different proportions during the synthesis process (The cross-sectional images of different PVDF membranes are shown in Figs. S2A-S2E in Supporting information). Under the optimal concentration of 15 % PVDF and 3 % PEG, the middle part of the section underwent a transition from a through-hole to a finger-like hole (Figs. S2F-S2G in Supporting information). The magnified view of internal pores at the micron level clearly revealed that the resultant membranes retained the homogeneous size and shape (Fig. S2H in Supporting information). Furthermore, the uniformity of the holes on the membrane surface illustrated its suitability for liquid mass transfer (Fig. S2I in Supporting information). Scanning electron microscope (SEM) mapping and energy-dispersive X-ray spectrometer (EDX) characterization illustrated that the composition of PVDF includes elements C and F (Fig. S3 in Supporting information).

To ensure efficient biofluid flow through the PVDF membrane, improving its hydrophilicity is essential. Hydrophilicity not only facilitates the smooth passage of biofluids but also imparts antifouling properties to the membrane, which is essential for maintaining its performance over time. The pure PVDF membrane had a water contact angle (WCA) of 93.61°, which remained stable for 6 min when a 10 μL water droplet was placed on the porous surface (Fig. 2A). This hydrophobic behavior is attributed to the intrinsic properties of unmodified PVDF, which can hinder biofluid flow and lead to membrane fouling during applications. To address this limitation and improve biofluid flux, a simple yet effective strategy was adopted by applying a composite coating of TP and APTES onto the PVDF membrane. The TP-APTES modification significantly enhanced the membrane's hydrophilicity. Water droplets were gradually absorbed when dropped on the TP-APTES/PVDF membrane within 40 s, confirming the porousness and hydrophilicity of the TP-APTES modified PVDF (Fig. 2B). This rapid absorption is a clear indication of the successful transformation of the membrane's surface properties from hydrophobic to hydrophilic.

To further enhance the antifouling property of the biosensor, a zwitterionic PEPG with a strong hydrophilicity was modified on the electrode surface. Here, two naphthalene groups (Nap) in the peptide 2-Nap-K-(2-Nap)-KF provided π-π accumulation force to form the transparent hydrogel (Fig. 3A) [32]. To endow the hydrogel self-healing capability, the strong π-π stacking force was provided by the 2 dimensions nanomaterial rGO to prepare rGO/PEPG (Fig. 3B) [32]. Remarkably, the rGO/PEPG cut into segments can self-healed within 5 min (Fig. 3C). SEM and transmission electron

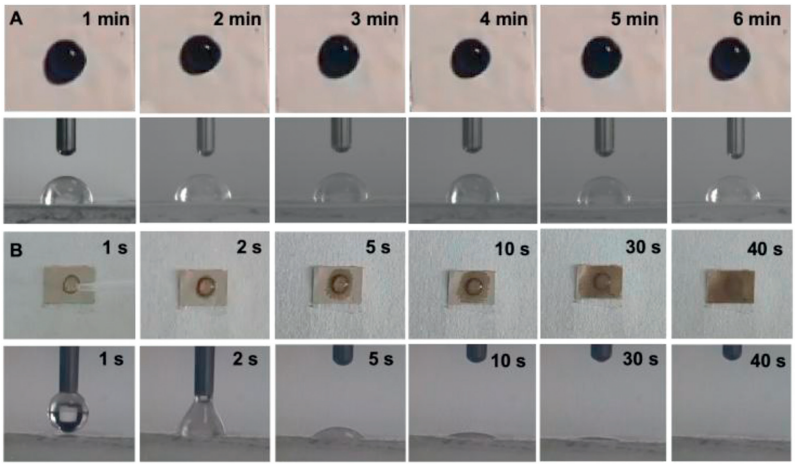


Fig. 2. Images of water drops on the membranes of PVDF (A) and TP-APTES modified PVDF membrane (B).

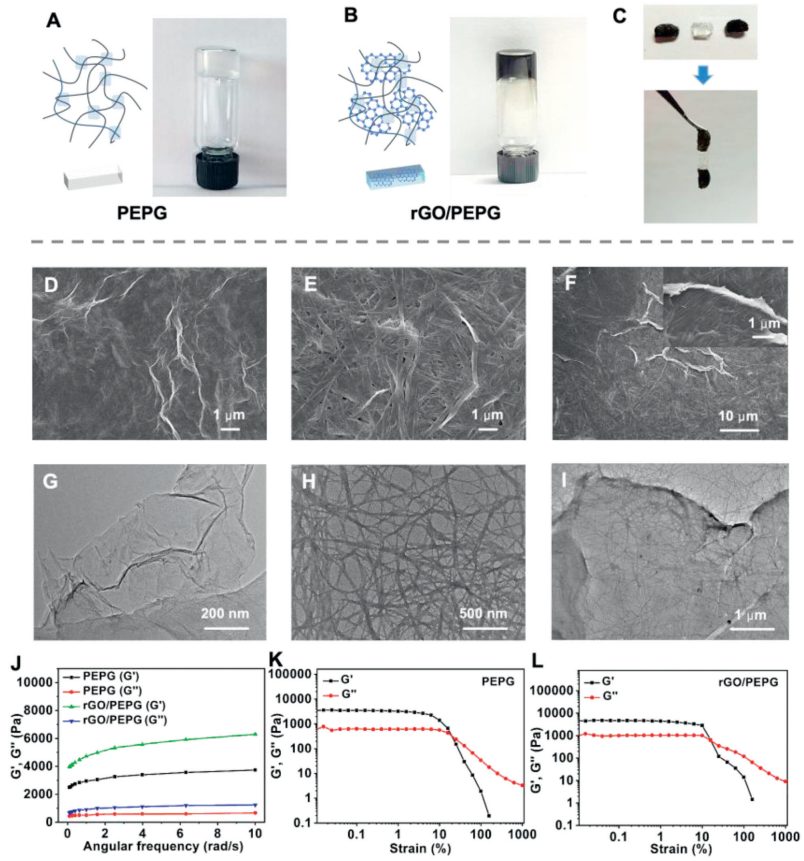


Fig. 3. The images of PEPG (A), rGO/PEPG (B), and the self-healing process of the rGO/PEPG (C). The SEM (D, E, F) and TEM (G, H, I) images of rGO (D, G), PEPG (E, H) and rGO/PEPG (F, I). (J) Frequency-dependent oscillatory rheology of the PEPG and rGO/PEPG, and the strain sweep analysis of the PEPG (K) and rGO/PEPG (L).

microscope (TEM) were employed to explore the micromorphology of the relevant materials involved. The SEM (Fig. 3D) and TEM (Fig. 3G) images of rGO unveiled a distinct morphology of undulating ripples reminiscent of silk veils at the micron scale. The PEPG exhibited a dense nanoscale network of linked nanofibers (Figs. 3E and H). With the introduction of rGO or gold nanoparticles and rGO composite material (AuNPs/rGO) into PEPG, the rGO or AuNPs/rGO was incorporated in the hydrogel and connected with the peptide fiber *via* the strong π-π stacking force, and the morphology of rGO or AuNPs/rGO and peptide fiber was remained, as depicted in Figs. 3F and I, Fig. S4 (Supporting information). And the sorption isotherm of rGO/PEPG showed a significant increase in N_2 adsorption at very high relative pressures ($P/P_0 > 0.9$), suggesting the presence of macro/supermacropores in the material (Fig. S5A in Supporting information). Nitrogen (N_2) adsorption-desorption analysis results also illustrated porous structure of rGO/PEPG with mesoporous and macropore (Fig. S5B in Supporting information), which is in favour of adsorption of much water molecules to resist biofouling.

The mechanical characteristics of the PEPG and rGO/PEPG, after being stored at 4 °C for 2 h, were assessed using the frequency-dependent oscillatory rheology. The results revealed that both the storage modulus (G') and loss modulus (G") were largely frequency-independent. The rGO/PEPG exhibited a higher G' value,

around 6 kPa, compared with that of the PEPG approximately 3.5 kPa (Fig. 3J), indicating that the introduction of rGO enhanced the mechanical strength of the PEPG. Additionally, the incorporation of rGO slightly increased the crosslink density within the hydrogel network. Both hydrogels displayed an extensive linear viscoelastic region and a noticeable breakage strain. In the strain amplitude sweep tests, G' and G" remained almost constant in the low-strain region (about 10 %). However, a critical strain of ~30 % triggered a gel-to-liquid transition, with the G' initially surpassing G" before falling below it. This critical strain point signified the transition from gel to liquid (Figs. 3K and L).

Considering that the electrical activity and antifouling properties of the composite materials are highly dependent on the combinations between rGO, PEPG, and AuNPs, and optimizing these ratios is crucial for achieving the best performance. In our study, we systematically evaluated different combinations of rGO and PEPG to determine the optimal ratio that balances electrical conductivity and antifouling properties. Specifically, we prepared a series of rGO/PEPG composites with varying concentrations of rGO (ranging from 1 mg/mL to 6 mg/mL) while keeping the concentration of PEPG constant. The electrical conductivities and the antifouling properties of each composite was measured using differential pulse voltammetry (DPV) technology. Our results indicated that a 5 mg/mL rGO to PEPG ratio provided the best compromise, offering high electrical activity while maintaining relatively low signal suppression rate compared with 6 mg/mL rGO. The reason is that the gradually increasing amount of rGO (1–5 mg/mL) progressively enhances the conductivity of the hydrogel. However, an excessive amount of the material (6 mg/mL) will lead to overlapping of the material's surface area, which in turn is detrimental to the hydrogel's conductivity. However, due to the low surface energy of rGO, with the gradual increase of rGO (1–5 mg/mL), the antifouling performance is also slightly increased. Excessive rGO (6 mg/mL) may lead to aggregation, resulting in an uneven surface structure that increases the adsorption sites for pollutants. Additionally, an overabundance of rGO can disrupt the hydrogel's network structure, compromising its overall performance, including its antifouling capabilities. Taking into comprehensive consideration, this combination of 5 mg/mL rGO and PEPG ensured sufficient conductivity for sensing applications while minimizing nonspecific adsorption, which is critical for biofouling resistance (Fig. S6A in Supporting information).

Regarding the combination of AuNPs with the rGO/PEPG hydrogel, we explored different deposition cycles of AuNPs (ranging from 1 to 4 cycles) using an electrochemical deposition method. The AuNPs were deposited onto the rGO/PEPG hydrogel by applying in a solution containing $HAuCl_4$. The electrical conductivity of the AuNPs-modified rGO/PEPG hydrogel was further evaluated using DPV technology, which showed a significant signal increase over 90 % after AuNPs 1 cycle deposition. This enhancement in conductivity is attributed to the excellent conductive properties of AuNPs, which facilitates electron transfer across the composite material. An appropriate and uniformly dispersed amount of AuNPs may enhance the antifouling properties of PEPG (1–3 cycles). However, excessive or unevenly distributed AuNPs could reduce antifouling performance, primarily due to aggregation effects or unfavorable alterations in surface properties (4 cycles, Fig. S6B in Supporting information).

Considering the complexity of human blood, it is imperative to investigate the antifouling performances of electrochemical sensors to be performed in this body fluid. We initially tested the antifouling properties of different electrodes by DPV technology, as the biofouling or nonspecific adsorption on the electrode surfaces when they are soaked in human blood will lead to decreases of the DPV peak currents. Different electrodes were incubated in various contents (5 %−50 %) of human blood for 30 min, respectively, and after incubation, the DPV of these electrodes were recorded in 5.0 mmol/L $[Fe(CN)_6]^{3-/4-}$ solution (containing 10 mmol/L PBS and 0.1 mol/L KCl). Notably, significant reductions (over 50 % signal suppression) in the DPV peak current and large DPV peak potential shifts were observed for the bare SPE when exposed to different human blood samples, indicating the heavy biofouling on the electrode surface that impeded the electron transfer (Fig. 4A, yellow color in Fig. 4D). In contrast, slight biofouling was observed for the peptide modified electrode and the biosensor based on the filtering-antifouling sandwich patch. Specifically, more than 20 % DPV signal suppression was found for the rGO/PEPG/SPE in 50 % human blood (Fig. 4B, green color in Fig. 4D). Interestingly, the biosensor with both the filtering and antifouling membranes exhibited excellent antifouling capability of about 10 % signal suppression rate even in 50 % human blood (Fig. 4C, blue color in Fig. 4D). As shown in the insets of Fig. 4D, after tangential flow filtration of the whole blood (red and opaque) by the PVDF filtering membrane, clear and light yellow human serum was obtained (Figs. 4E and F). This effective blood filtration ability of the PVDF membrane is believed to enhance the antifouling capability of the biosensor. Moreover, the prepared PVDF filtering membrane can be recycled after simple cleaning with water (Figs. 4G-I).

To gain a deeper understanding of the non-specific biofouling adsorption phenomenon and devise a strategy to address the biofouling issues of modified electrodes, the WCA and confocal microscopy were afterward utilized to evaluate the relationship between hydrophilicity of modified electrodes and efficacy of preventing fluorescein isothiocyanate-labeled bovine serum albumin (FITC-BSA) adsorption on various modified electrode surfaces. Generally, good hydrophilicity means excellent antifouling properties. For example, the relatively large WCA of 117.19° (Fig. 5A) and significantly high fluorescence intensity on the bare SPE surface (Figs. 5A1-A3) indicated weak antifouling properties. Similarly, the relatively higher WCA of 46.90° (Fig. 5B) and fluorescence intensity meant the poorer antifouling ability of rGO (Figs. 5B1-B3). Conversely, the rGO/PEPG surface showed barely visible fluorescence due to its excellent antifouling properties attributed to PEPG's hydrophilicity with WAC of 10.91° (Fig. 5C) and its electric neutrality (Figs. 5C1-C3).

According to our requirement, a novel biosensor for cortisol bioassay was designed (Fig. 6A). Cortisol, a key stress hormone secreted by the adrenal glands, plays a vital role in regulating metabolism, immune response, and stress adaptation. Abnormal cortisol levels are associated with various disorders, such as Cushing's syndrome (high cortisol) and Addison's disease (low cortisol). Regular detection of cortisol levels helps in early diagnosis of these diseases, guiding appropriate treatment strategies. It also aids in assessing the body's stress response in different physiological and pathological conditions, providing valuable insights for maintaining overall health [33–35]. The DPV technology was used to evaluate the sensing process of each modified steps in a solution of 5.0 mmol/L $[Fe(CN)_6]^{3-/4-}$ solution (containing 10 mmol/L PBS and 0.1 mol/L KCl). In feasibility details of the developed biosensor, working electrode was fabricated by coating rGO/PEPG through π-π stacking force with a minimum peak (black line, Fig. S7 in Supporting information). And AuNPs functionalized rGO/PEPG was to facilitate the efficient electron transfer (red line, Fig. S7). And AuNPs were used as the excellent immobilization matrix with aptamers through Au-S bonds. However, in the presence of aptamers and the target cortisol (1 ng/mL), the signal gradually decreased in sequence because of aptamers and cortisol's weak electrical conductivity (blue line and purple line, Fig. S7). And electrochemical impedance spectroscopy (EIS) showed the opposite results to illustrate the developed biosensor's feasibility (Fig. S8 in Supporting information). Therefore, the sensing activity of the cortisol detection ensures the feasibility of the biosensor.

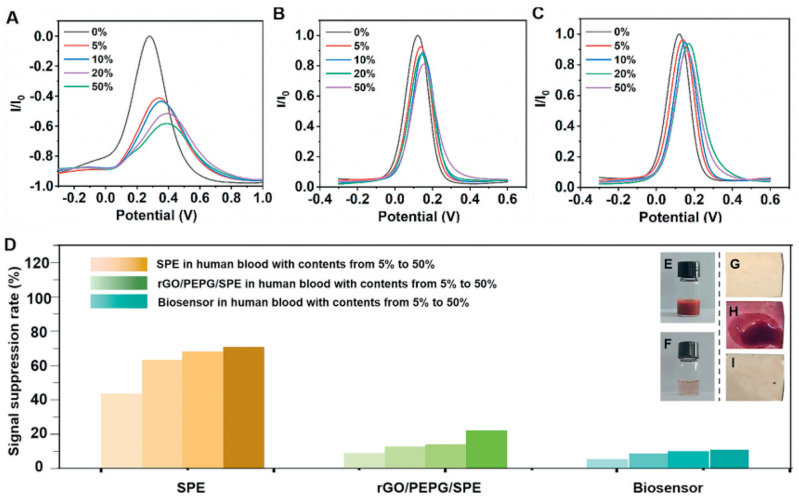


Fig. 4. The DPV response curves of the bare SPE (A), rGO/PEPG/SPE (B) and the biosensor based on the sandwich patch (C) after soaking in various human blood samples for 30 min. (D) Antifouling performances of different electrodes in various contents of human blood for 30 min (the colors from light to dark represent 5%, 10%, 20%, and 50% human blood, respectively). The images of 50% cattle blood before (E) and after (F) filtration by the prepared PVDF filtering membrane. The images of TP-APTES modified PVDF membrane before (G), after (H) soaking in cattle blood, and the image of the TP-APTES modified PVDF membrane after cleaning the contaminated membrane by cattle blood (I).

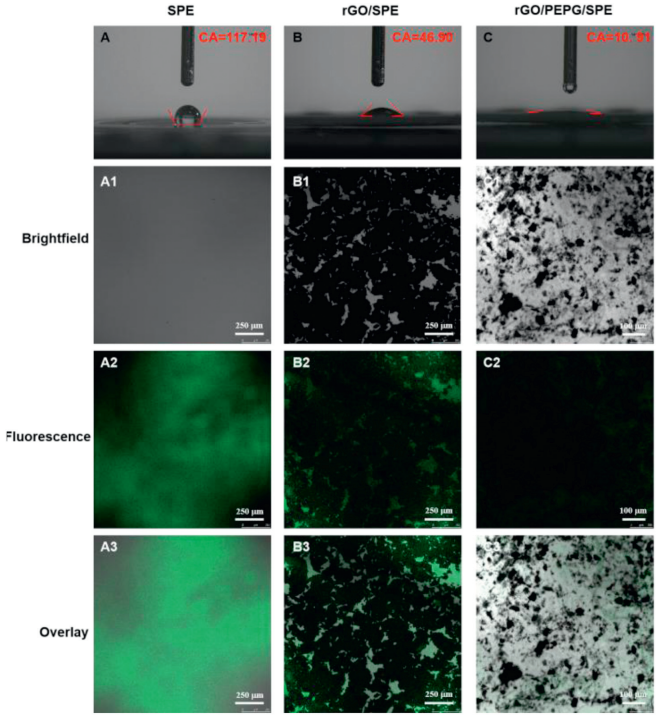


Fig. 5. The water contact angles of the bare SPE (A), and rGO (B) and rGO/PEPG/SPE (C). The fluorescence images of (A1-A3) SPE, and (B1-B3) rGO and (C1-C3) rGO/PEPG/SPE.

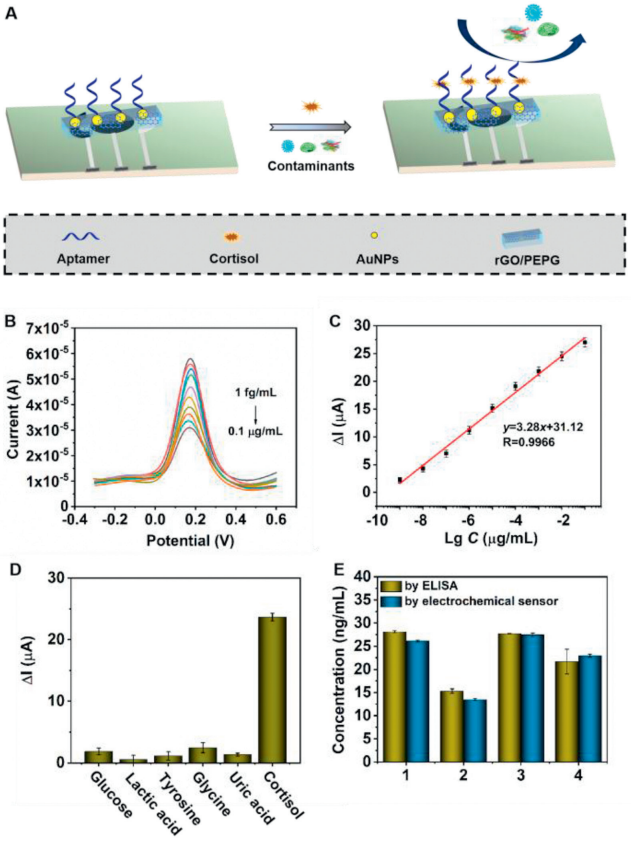


Fig. 6. (A) The sensing scheme of the biosensor for cortisol detection. The detection of cortisol in PBS (B). The linear range of the biosensor performed in PBS (C). (D) The DPV signal changes of biosensor for different potential interferents (100 ng/mL) and cortisol (10 ng/mL). (E) The concentrations of free cortisol in 4, 20% human blood samples measured by both the ELISA method and the proposed sensor.

Cortisol detection efficacy was tested in phosphate buffered solution (PBS) across a range of concentrations (Figs. 6B and C). As the cortisol levels increased, corresponding changes in DPV (ΔDPV) were noted, covering concentrations from 1 fg/mL to 0.1 μg/mL (Fig. 6B, Fig. S9 in Supporting information). The calibration curve displayed a linear correlation between ΔI and cortisol concentration within this range (Fig. 6C). The resulting linear equation was $\Delta I = 31.12 + 3.28$ LgC, with a coefficient of determination (R) of 0.9966. The detection limit for the cortisol assay was notably low, reaching 0.33 fg/mL (S/N = 3). The biosensor has shown the excellent selectivity (Fig. 6D) and reproducibility (Fig. S10 in Supporting information). The specificity of the biosensor was assessed by measuring its response to 10 ng/mL cortisol. Subsequently, 100 ng/mL glucose, lactic acid, tyrosine and uric acid were tested as control (Fig. 6D). The results revealed a distinct and significant reaction to low concentrations of cortisol, while

negligible responses were observed for higher concentrations of other potentially interfering substances. This indicated the antifouling biosensor's remarkable selectivity and specificity. Additionally, the reproducibility of the biosensor was verified using five independent sensors with 0.1 μg/mL cortisol (Fig. S10). The low relative standard deviation (RSD) of 1.34 % among the five biosensors confirmed its superior reproducibility. And the accuracy of the electrochemical sensor was evaluated using 20 % human blood samples for free cortisol concentration detection from 4 volunteers, comparing its performance against commercial ELISA kits. The ELISA kit is a highly sensitive detection tool widely used in biomedical research, clinical diagnostics, and drug development. It is based on the principle of specific antigen-antibody binding and utilizes enzyme-labeled technology to combine immune reactions with enzyme-catalyzed reactions, enabling the quantitative or qualitative detection of target molecules through colorimetric or fluorescent signals. It is suitable for various sample types, such as serum, plasma, cell culture supernatants, and more. The operation is relatively simple, and the results are stable and reliable. Because the potential denaturation or hydrolysis of the aptamer when applied to real blood in the sensing layer is a crucial issue. So, we have conducted preliminary stability tests in real castle blood. We incubated the aptamer-immobilized sensing layer in real castle blood for several time. Through electrochemical method, the signal suppression rate changes under 10 % within 8 h. The results showed that within the detection time frame and under the experimental conditions we set, the aptamer maintained a relatively stable state, and there was no significant denaturation or hydrolysis observed (Fig. S11 in Supporting information). So, our biosensor also can be used in blood samples. As illustrated in Fig. 6E, the cortisol concentration measurements from our sensor closely matched those from the ELISA kits, demonstrating the sensor's precision.

We also conducted additional experiments to assess the sensor's performance after extended storage periods of 0.5, 2, 18, 19 h and the detection under 0, 25, 37 °C, and under the complex testing sample with adding 10 mmol/L BSA in sensing sample. These results showed signal stability under various complex environment and under 18 h of storage time (Fig. S12 in Supporting information). These results will provide a more comprehensive evaluation of the sensor's stability and practical applicability.

In this work, we developed an innovative approach to overcome heavy biofouling on sensor surfaces by creating an advanced antifouling electrochemical sensor with dual antifouling mechanisms. The antifouling layer **1**, a porous membrane with robust hydrophilicity and size effect, efficiently filters out micron-sized contaminants. The antifouling layer **2**, the rGO/PEPG, maintains electric neutrality and features self-healing properties, enhancing antifouling performance. Using this filtering-sensing sandwich patch, we successfully detected cortisol in human blood, demonstrating the sensor's effective functionality in complex biological fluids. This innovative design, incorporating precise control over pore size and hydrophilicity, enables biosensors to perform robustly in complex human body fluids.

Ethical statement

The blood samples were provided from Qingdao Central Hospital. All sample preparations were approved by the relevant Institutional Review Committee and carried out in accordance with institutional guidelines and conformed to the relevant regulatory ethical standards.

Declaration of competing interest

The authors declare that they have no known competing financial interests or personal relationships that could have appeared to influence the work reported in this paper.

CRediT authorship contribution statement

Xiujuan Qiao: Writing – original draft, Investigation, Data curation, Methodology, Funding acquisition. **Rui Han:** Writing – review & editing, Formal analysis. **Xinru Xu:** Methodology. **Mingrui Lv:** Data curation, Formal analysis. **Yiting Hou:** Data curation, Formal analysis. **Xiliang Luo:** Supervision, Methodology, Data curation, Writing – review & editing, Project administration, Funding acquisition.

Acknowledgments

This work was supported by the National Natural Science Foundation of China (Nos. 22174082, 22374085), the Key Research and Development Program of Shandong Province (No. 2021ZDSYS30), and Natural Science Foundation of Shandong Province, China (No. ZR2024QB059).

Supplementary materials

Supplementary material associated with this article can be found, in the online version, at doi:10.1016/j.cclet.2025.111598.

References

[1] C. Ye, H. Lukas, M. Wang, et al., Chem. Soc. Rev. 53 (2024) 7960–7982.
[2] M. Li, X. Wang, Y. Zhu, et al., Chin. Chem. Lett. 34 (2023) 107299.
[3] Z. Song, R. Li, X. Yang, Chin. Chem. Lett. 34 (2023) 108314.
[4] J. Liu, Y. Lu, Y. Hu, et al., Anal. Chem. 96 (2024) 5546–5553.
[5] C. Liu, X. Lin, J. Liao, Chin. Chem. Lett. 4 (2024) 109598.
[6] M. Sun, X. Pei, T. Xin, et al., Anal. Chem. 94 (2022) 1890–1900.
[7] Z.Q. Wu, X.Q. Cao, Y. Hua, et al., Anal. Chem. 96 (2024) 3087–3095.
[8] C. Jiang, G. Wang, R. Hein, et al., Chem. Rev. 120 (2020) 3852–3889.
[9] Z. Song, R. Li, Z. Li, et al., Biosens. Bioelectron. 264 (2024) 116640.
[10] H. Chen, Z. Wang, Z.L. Song, et al., Anal. Chem. 96 (2024) 3233–3242.
[11] S. Gu, X.M. Shi, D. Zhang, et al., Anal. Chem. 93 (2021) 2706–2712.
[12] X. Qiao, Z.H. Qian, W. Sun, et al., Anal. Chem. 95 (2023) 11091–11098 b.
[13] w.A. Al-Soud, P. Radstrom, J. Clin. Microbiol. 39 (2001) 485–493.
[14] J. Durner, Angew. Chem. Int. Ed. 49 (2010) 1026–1051.
[15] D. Mabey, R.W. Peeling, A. Ustianowski, et al., Nat. Rev. Microbiol. 2 (2004) 231–240.
[16] Z. Chu, W. Zhang, Q. You, et al., Angew. Chem. Int. Ed. 59 (2020) 18701–18708.
[17] B. Charra, E. Calemard, M. Ruffet, Kidney Int. 41 (1992) 1286–1291.
[18] L. Deng, J. Liu, Y. Chen, et al., Chem. Eng. J. 497 (2024) 154641.
[19] B.B. Berking, G. Poulladofonou, D. Karagrigoriou, et al., Angew. Chem. Int. Ed 62 (2023) E202308971.
[20] D. Chan, J.C. Chien, E. Axpe, et al., Adv. Mater. 34 (2022) 2109764.
[21] D. Karagrigoriou, B.B. Berking, Q. Wang, et al., ACS. Macro Lett. 12 (2023) 1608–1613.
[22] J.F. Karthäuser, R. Kopecz, E. Schönemann, et al., Adv. Mater. Interfaces. 11 (2024) 2300873.
[23] P. Sarker, T. Lu, D. Liu, et al., Chem. Sci. 14 (2023) 7500–7511.
[24] T. Yagasaki, N. Matubayasi, Langmuir 40 (2024) 15046–15058.
[25] A. Zardehi-Tabriz, Y. Ghayebzadeh, A.E. Gerdroodbar, et al., Macromol. Mater. Eng. 308 (2023) 2300179.
[26] K. Neumann, Biomater. Sci. 12 (2024) 5481–5490.
[27] S. Moayedi, W. Xia, L. Lundergan, et al., Langmuir 40 (2024) 23125–23145.
[28] J. Zhao, Q. Liu, X. Tong, et al., Adv. Funct. Mater. 34 (2024) 2401466.
[29] Y. Wang, W. Zhang, C. Gong, et al., Soft. Matter. 16 (2020) 10029–10045.
[30] Q. Wang, C. Jiao, X. Wang, et al., Biosens. Bioelectron. 221 (2023) 114908.
[31] E.S. Lee, M.Y. Lee, D.H. Kim, et al., Adv. Eng. Mater. 26 (2024) 2401432.
[32] X. Qiao, Y. Cai, Z. Kong, et al., ACS. Sens. 8 (2023) 2834–2842 a.
[33] B.R. Walker, Diabet. Med. 23 (2006) 1281–1288.
[34] A. Barthel, G. Benker, K. Berens, et al., Exp. Clin. Endocr. Diab. 127 (2019) 165–175.
[35] D.Y. Lee, E. Kim, M.H. Choi, BMB Rep. 48 (2015) 209.